APPLICATION OF THE CONSTRAINED ADMISSIBLE REGION MULTIPLE HYPOTHESIS FILTER TO INITIAL ORBIT DETERMINATION OF A BREAK-UP

Tom Kelecy[(1)], Michael Shoemaker[(2)], Moriba Jah [(3)]

[(1)] The Boeing Company, 5555 Tech Center Drive, Ste. 400, Colorado Springs, CO 80919, USA, Email: Thomas.M.Kelecy@boeing.com
[(2)] Los Alamos National Laboratory (LANL), ISR-1, MS D466, Los Alamos, NM 87545, USA, Email: Shoemaker@lanl.gov
[(3)] Air Force Research Laboratory (RV), 3550 Aberdeen Ave., SE, Kirtland AFB, NM 87117, USA

ABSTRACT

A break-up in Low Earth Orbit (LEO) is simulated for 10 objects having area-to-mass ratios (AMR's) ranging from 0.1-10.0 m^2/kg. The Constrained Admissible Region Multiple Hypothesis Filter (CAR-MHF) is applied to determining and characterizing the orbit and atmospheric drag parameters (CdA/m) simultaneously for each of the 10 objects with no *a priori* orbit or drag information. The results indicate that CAR-MHF shows promise for accurate, unambiguous and autonomous determination of the orbit and drag states.

1 INTRODUCTION AND BACKGROUND

The vast majority of space objects (SO's) orbiting the earth are uncontrolled. Of the SO's in Low Earth Orbit (LEO), some as yet undetermined number of these have dynamic perturbation components that are not completely predictable and, when combined with their dim, time-varying visual magnitudes, make them difficult to track consistently. Additionally, when a new break-up occurs there are numerous "new" observation tracklets that must be associated, and the orbit and drag states determined for the tracked objects. Initially sparse tracking data make follow-up determination of the orbit and atmospheric drag parameters a challenge, and even when tracked consistently, erroneous assumptions regarding the statistical distribution of the errors can exacerbate the challenge of data association and subsequent attempts to accurately compute conjunction assessments.

Previous work [1] demonstrated the viability of using a Constrained Admissible Region-Multiple Hypotheses Filter (CAR-MHF) to perform initial state estimation (ISE) using sparse data collected on a high area-to-mass ratio (HAMR) SO orbiting in a near geosynchronous orbit (GEO).

This work applies the CAR-MHF to simulated tracking data representative of a break-up in LEO to determine its viability for use in that orbit regime. Optical tracking data from a ground station are simulated for 10 objects originating from a single host object, and CAR-MHF is used to initialize tracks and associated hypotheses which include orbit and drag parameters. The subsequent data (i.e. obtained on follow-up passes over the ground site) are associated to determine the orbit states. The resulting estimated orbit and drag parameters, and data association statistics, are compared to the known "truth" orbits and the results presented. The approach accommodates the orbit determination of spatially and temporally distributed objects having a range AMRs.

2 CONSTRAINED ADMISSIBLE REGION MULTIPLE HYPOTHESIS FILTER

The CAR-MHF algorithms support initialization of orbit and parameters states without any specific *a priori* state information beyond general orbit constraints (e.g. neighbourhood of LEO regime). A probabilistic data association scheme is applied for one or more measurements at a given time to hypothesized orbits to determine which hypotheses are the most likely candidates. CAR-MHF has been described in more detail in [2, 3]. This section provides a summary of the conceptual background and the implementation relevant to this work.

Milani [4] initially used the Admissible Region to aid in determining orbits of asteroids, and DeMars et al. [3] extended it for determining orbits for Earth-orbiting objects. Figure 1-a illustrates an example of the range, range-rate solutions for a set of near GEO semi-major axis (left) and eccentricity (right) constraints, where a Keplerian orbit is assumed. Each line represents solutions for a specific constraint value. Figure 1-b presents an example of the super-position of a single set of semi-major axis and eccentricity constraints (left) and the region of intersection (right) for each of the constraints. This is the 'CAR' which, when discretized, results in the set of range and range-rate pairs; these pairs are then combined with angle and angle rate measurements to derive the hypothesized states.

Proc. '6th European Conference on Space Debris'
Darmstadt, Germany, 22–25 April 2013 (ESA SP-723, August 2013)

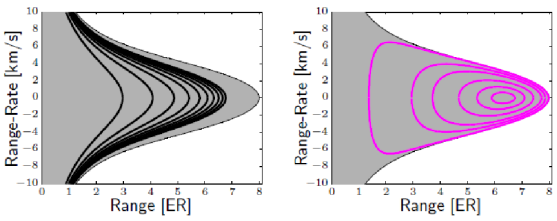

Figure 1-a. Range vs. Range-rate near GEO semi-major axis (left) and eccentricity (right) constraints.

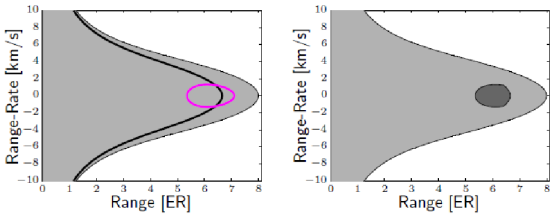

Figure 2-b. Intersection of a given set of near GEO semi-major axis and eccentricity constraints (left) and the remaining Constrained Admissible Region (right).

The measurements and their associated *a priori* uncertainties (derived from the measurement noise) can be combined with the hypothesized range and range-rate pairs, and *a priori* covariances derived from their discretized spacing, to form a six element state and associated covariance. These hypothesized measurement states, along with their mean, can be mapped via the Unscented Transform (UT) to form a set of hypothesized and mean Cartesian positions and velocities and their associated *a priori* covariances [5]. This process is illustrated in Figure 2.

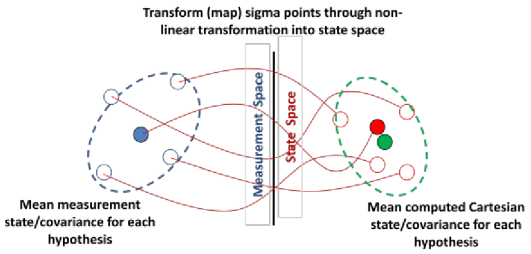

Figure 2. A sigma point transform is used to map the angle, angle rate, range and range-rate to Cartesian position and velocity coordinates for each hypothesis.

The process just described results in a set of hypothesized orbit states. However, if ballistic coefficient (BC) is also hypothesized, these hypothesized values must also be added to the overall set of hypotheses. This is done via a set of user-defined values specifying a set of hypothesized SRP and/or BC values. As with the hypothesized states, the *a priori* covariances associated with these state components are derived from the spacing between the hypothesized values.

3 SIMULATION OF LEO BREAK-UP

A break-up was simulated consisting of 10 "pieces" emanating from a single LEO satellite position at a specific time. A nominal orbit having a semi-major axis of 7000 km, eccentricity of 0.01, and inclination of 45 degrees was used. A dispersion of 10 m/s (1-σ) for the Δv's was added to the nominal orbital velocity for modelling the break-up, in addition to randomly selecting initial BC (i.e. CdA/m) values over the interval 0.01-10.0 m^2/kg. The BC of each satellite fragment was kept constant in time for this simulation. This purpose of using this simple non-energy preserving break-up model was to validate CAR-MHF suitability for LEO data processing, and to assess data association and processing performance.

A "truth" trajectory was generated using a 6x6 EGM 96 Earth gravity model, sun and moon third body gravitation, and drag acceleration. The low degree and order Earth gravity were used for this initial demonstration study to expedite processing. Filter and "truth" models used for the measurement simulation were consistent. Right ascension and declination measurements were simulated in tracklets spanning several minutes and the measurement intervals separated by about 60 seconds for a sensor location in New Mexico. The measurements were corrupted with a one arc-sec (1- σ) additive Gaussian white noise error.

A plot of the dispersing objects at a specific moment in time, primarily in the in-track component, is shown in Figure 3, and the BC values that were generated for the 10 debris objects are provided in Table 1. Measurement tracklets consisting of a set of topocentric right ascension and declination angles for a sensor located in New Mexico, USA, were simulated over a span of 3 days, with visibility constraints applied.

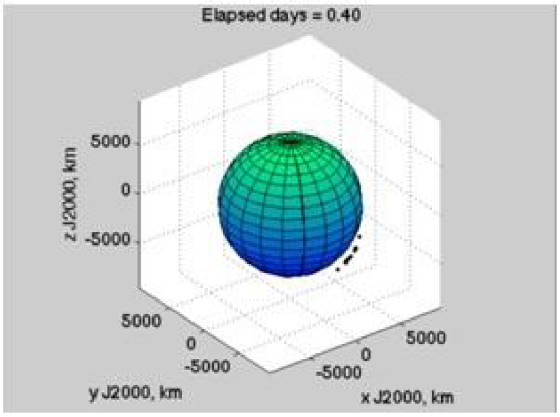

Figure 3. Snapshot in time of the 10 simulated LEO debris objects dispersing in the in-track direction.

Another assumption made in this study is that the probability of detection for any given object within the visibility constraints is equal to one. In addition to the range of BC's, Table 1 also includes the starting number of hypotheses, number of hypotheses at convergence, the time (i.e. in simulation time, not computer run time) and number of observation updates to convergence. All but one of the objects converged to a single hypothesis in less than 2 hours (44-56 measurement updates), while object #8 took nearly 8 hours and 163 measurements to converge. This is the result of the BC value being nearly 5 m^2/kg which is nearly mid-way between the two hypothesized AMR values of 0.01 m^2/kg and 10 m^2/kg that were used. It was simply the result of the MHF needing more time and data to decide on the final value due to the filter having farthest to go for convergence to that particular value.

Table 1. Drag and hypothesis history for the 10 simulated LEO debris objects.

Object #	CdA/m (m^2/kg)	Start Hypoth. #	End Hypoth. #	Conv. Obs. #	Conv. Hours
1	8.691	134	1	56	1.8
2	0.405	142	1	56	1.8
3	0.017	130	1	47	1.7
4	6.308	134	1	44	1.7
5	2.564	136	1	47	1.7
6	1.205	138	1	48	1.7
7	3.107	122	1	47	1.7
8	4.471	124	1	163	7.8
9	0.300	140	1	56	1.8
10	7.661	148	1	48	1.7

4 CAR-MHF PROCESSING

The CAR-MHF processing is illustrated in Figure 4. The CAR process initiates a set of filters when no existing estimates are available to process. Existing estimates may be available from previous CAR generations. The CAR initiates a set of hypotheses based on an un-associated tracklet of data and user supplied hypothesis constraints. Each hypothesis is propagated to the next measurement time. At that point, a probabilistic data association process is applied to one or more data pairs that might occur at a single time. If any measurements are associated to any hypotheses (based upon a Mahalanobis Distance criterion), all hypotheses are updated for the associated measurement, and those updated are weighted based on their statistical likelihood as presented in [3]. In the case of an update, the hypothesis weights are adjusted accordingly and pruned based on user-selected criteria. If no update occurs, the hypotheses weights remain unchanged.

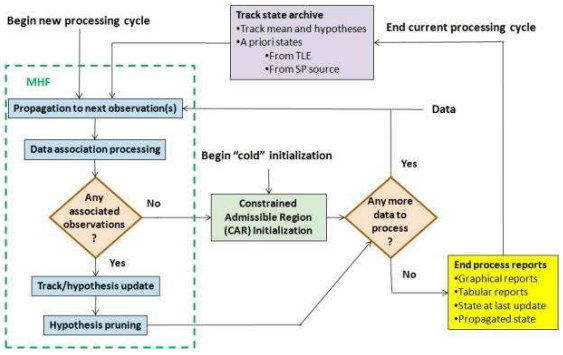

Figure 4. CAR-MHF process flow.

Conceptually, the data and hypothesis update approach enables multiple data to inform the filter which hypotheses are the most likely states. Each filter update further refines the hypotheses, rejecting the least likely, so ultimately the surviving hypothesis (or couple of hypotheses) is the converged state. This process is depicted in Figure 5, where it should be noted that the Mahalanobis distance metric is the basis for the data association. Each hypothesis state and covariance at the measurement time is mapped to measurement space ("C" and "P" in Figure 5) and compared to the measurement at that time ("O" in Figure 5). The k^2 parameter is a chi-squared statistic that is compared against a user-specified probability limit for the purpose of data association determination (and holds for distributions that are sufficiently Gaussian).

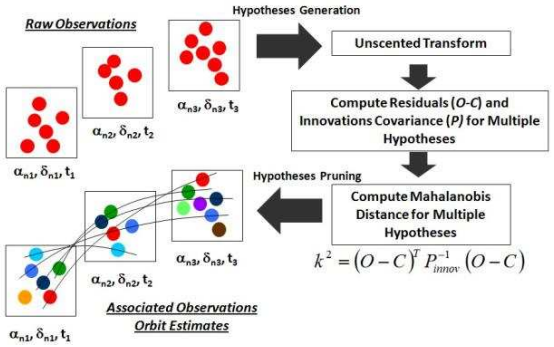

Figure 5. Conceptual depiction for multiple hypothesis and multiple data association processing.

Figure 6 shows an example for the discretized CAR for one of the simulated debris objects presented in orbital parameter space. The "dots" in the top, middle and bottom plots are each of the state hypothesis orbital components, plotted as eccentricity, inclination and right ascension of ascending node versus semi-major axis, respectively. There are additional corresponding hypotheses for argument of perigee and mean anomaly, and any drag hypotheses that the user has defined for the processing.

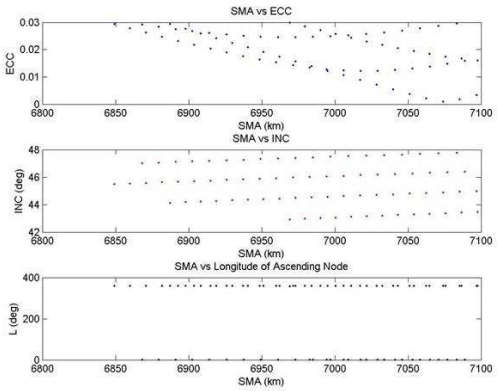

Figure 6. Sample hypotheses for one LEO debris object: semi-major axis, eccentricity, inclination and right ascension of ascending node.

Before moving on to analysis results, it should be noted that SRP and drag parameters can either be hypothesized, estimated, or both hypothesized and estimated. There may be situations where a parameter (e.g. SRP) might not be "observable" over a particular span of measurements, and so it might make more sense to initially hypothesize the parameter only, and eventually estimate it when subsequent data are made available.

Figure 7 shows an example from one of the simulated debris objects of the hypothesis history in terms of observation number. Hypotheses are "pruned" based on the weights that are adjusted to each of the hypotheses when a measurement update occurs, and the weights are based on the likelihood that a measurement is associated with a given hypothesis. The hypothesis pruning will be a function of measurement density, geometry, and the parameters being estimated, among other things.

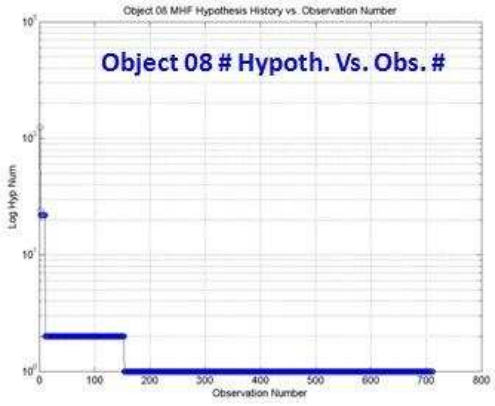

Figure 7. Hypothesis number history vs. observation update number for one LEO debris object.

5 ANALYSIS RESULTS

The CAR-MHF processing was applied to the 10 simulated debris objects, where a CAR (set of hypotheses) was initiated when a "tracklet" of data were encountered that had not previously been associated. A summary of the hypotheses histories was presented in Table 1 above, and all tracks converged to a single hypothesis.

Since the "truth" orbit and drag parameters were known for each of the 10 objects, they could be compared to the filter estimates at any given time. Figures 8 shows the total position error (red squares) and 3-sigma filter uncertainty (blue diamond's) for each of the 10 objects indicated by the integers 1 to 10 on the x-axis of the plot at the end of 1-day of processing. The position errors range from 2-5 meters, and these errors are bounded by filter uncertainties that are on the order of 8-9 meters. The corresponding drag parameters estimation errors and 3-sigma uncertainties after 1-day are given in Figure 9 for each of the 10 objects. The larger errors correspond to the objects having lower BC values, and this indicates longer time spans of data are needed for these to converge adequately.

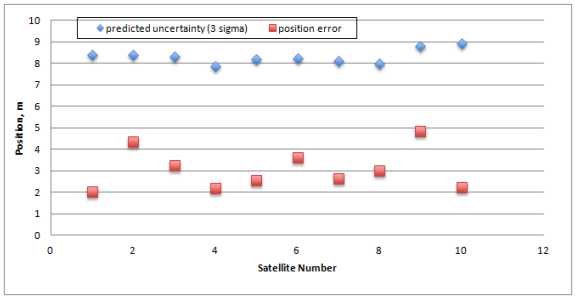

Figure 8. RSS of position errors (red squares) and 3-sigma estimation uncertainties (blue diamonds) for each of the 10 LEO debris objects after 1 day of processing.

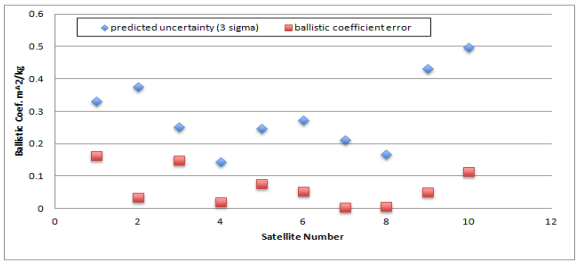

Figure 9. Drag errors (red squares) and 3-sigma estimation uncertainties (blue diamonds) for each of the 10 LEO debris objects after 1 day of processing.

Figures 10 and 11 are the position and drag errors and 3-sigma filter uncertainties for the 10 objects after 3-days of processing. The total position errors are seen to converge to better than 1-2 meters, while the drag

converges to better than a percent. Notice that the additional data have allowed the drag parameter to converge to acceptable accuracy for all of the BC values, including satellites with lower BC values.

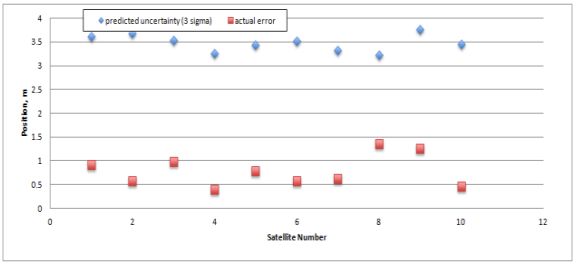

Figure 10. RSS of position errors (red squares) and 3-sigma estimation uncertainties (blue diamonds) for each of the 10 LEO debris objects after 3 days of processing.

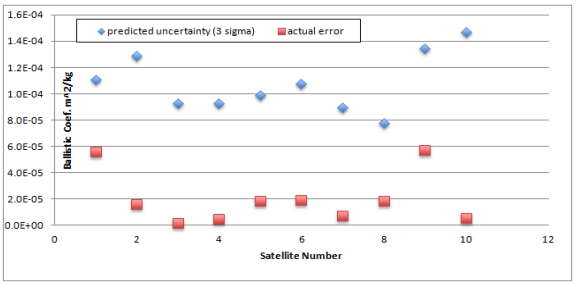

Figure 11. Drag errors (red squares) and 3-sigma estimation uncertainties (blue diamonds) for each of the 10 LEO debris objects after 3 days of processing.

Figures 12-15 present an example of the semi-major axis, inclination, eccentricity and drag estimate histories, respectively, for one of the 10 objects. Note that a large BC value results in a systematic decrease in semi-major axis, and that abundant data results in a rapid convergence of eccentricity and inclination. The drag converges to several percent after the first day, and to less than 1% by the end of the 3-day period.

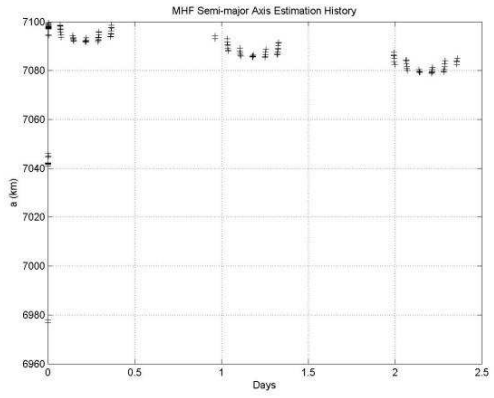

Figure 12. Semi-major axis estimation history for one of the LEO debris objects.

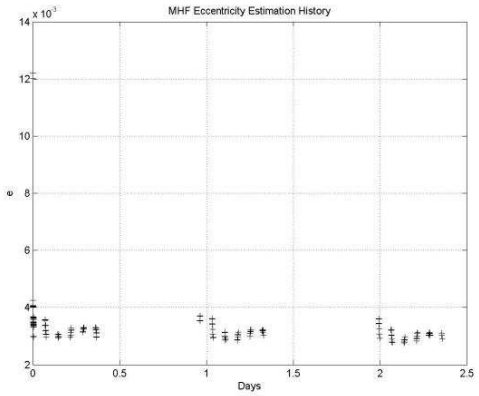

Figure 13. Eccentricity estimation history for one of the LEO debris objects.

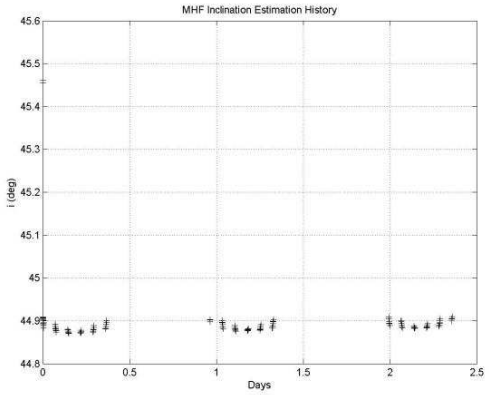

Figure 14. Inclination estimation history for one of the LEO debris objects.

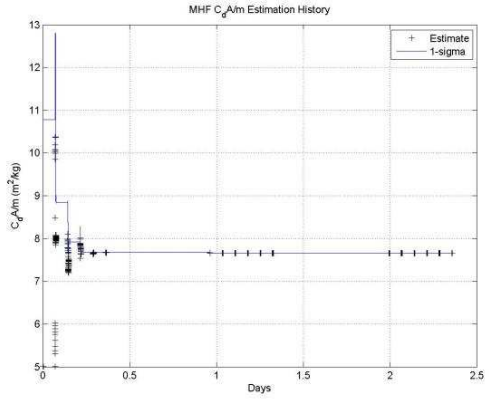

Figure 15. Drag BC (CdA/m) estimation history for one of the LEO debris objects.

The radial (blue), in-track (red) and cross-track (black) 1-sigma uncertainties for position and velocity are provided in Figures 16 and 17. The radial position converges to a few meters by the end of the 3-day

period, and the radial velocity to much better than 1 m/s. The covariance growth between measurement periods is evident in the plots.

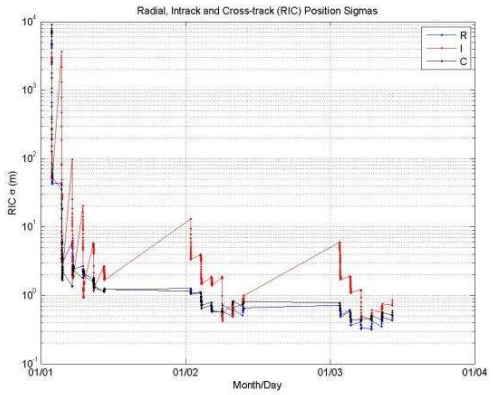

Figure 16. Radial, In-track and Cross-track 1-sigma position estimation uncertainty history for one of the LEO debris objects.

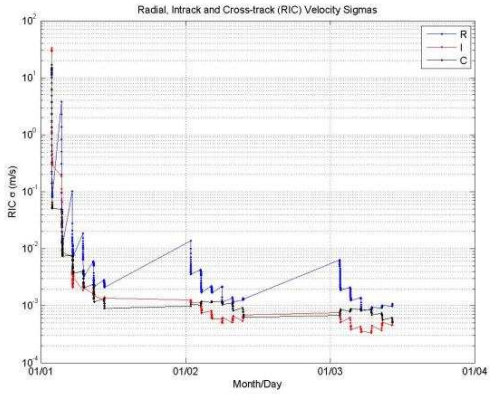

Figure 17. Radial, In-track and Cross-track 1-sigma velocity estimation uncertainty history for one of the LEO debris objects.

The plot of post-fit right ascension and declination residuals is shown in Figure 18, with the values consistent with the 1 arc-sec noise used in the simulation of the measurements.

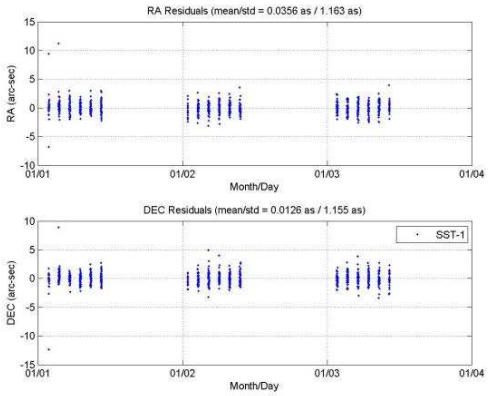

Figure 18. Right ascension and declination post-fit residual history.

6 SUMMARY AND CONCLUSIONS

A LEO break-up was simulated for 10 debris objects having a range of BC values, and CAR-MHF was used to initialize and characterize the orbit and drag states in an accurate, unambiguous and autonomous fashion. The results are viewed more as a validation of concept, and more development is needed to accommodate actual data.

Nevertheless, there were several things of value that can be concluded from this analysis. The filter convergence is sensitive to data cadences and the unique geometric diversity of the sensor location. One does not always have the luxury of ample data, so this can be made up for somewhat by smart sensor placement. It was also determined that, for CAR initialization, a quadratic fit in the tracklet data was better for rate determination due to the greater geometric structure resulting from the LEO orbit as compared to a GEO orbit where a linear fit is usually sufficient. It was also found that for a wide range of drag parameters, the drag needed to be hypothesized, in addition to being estimated, to accommodate the wide range of values and relatively large *a priori* uncertainties. Also, lower magnitude drag values required longer spans of data and time to converge accurately. Lastly, though the data association seemed to work fairly well for this limited data set, our experience indicates that in a more cluttered data environment other techniques will need to be applied, such as perhaps adding the angle rate to the data association processing.

Future implementations will include incorporation of Gaussian mixture models (AEGIS) [6] to account for non-Gaussian error characteristics. Incorporating feature-aided measurements (e.g. photometry), when available, should also help with the data association and hence improve filter accuracy and convergence. Further analysis needs to be conducted that includes SRP to insure it and the drag can be adequately separated in the

estimation processing. Including more accurate density models, and determining sensitivity to density model errors would also be of value.

The CAR-MHF process presents a potentially valuable tool for quickly and autonomously initializing and characterizing the orbits for numerous unknown and/or uncorrelated objects in LEO. This capability could be beneficial to the study of atmospheric space environment through dynamic characterization of spatially distributed space objects [7].

7 ACKNOWLEDGEMENTS

We would like to thank the Air Force Research Laboratory and Los Alamos National Laboratories for funding the research presented here.

8 REFERENCES

1. Kelecy, T., M. Jah and K. DeMars (2012). Application of a Multiple Hypothesis Filter to near GEO high area-to-mass ratio space objects state estimation. Acta Astronautica, 81, pp 435-444.

2. DeMars, K., M. Jah and P. Schumacher (2012). Initial Orit Determination using Short-Arc and Angle Rate Data. IEEE Journal of Transactions on Aerospace and Electronic Systems, Volume 48, Number 3, July 2012.

3. DeMars and K., M. Jah (2009). Passive Multi-Target Tracking with Application to Orbit Determination for Geosynchronous Objects. AAS Paper 09-108, 19th AAS/AIAA Space Flight Mechanics Meeting, Savannah, Georgia, February 8-12, 2009.

4. Milani, A., G. Gronchi, M.D.M. Vitturi and Z. Knezevic (2004). Orbit Determination with Very Short Arcs. I Admissible Regions. Celestial Mechanics and Dynamical Astronomy, Vol. 90, July 2004, pp59-87.

5. Julier, S. and J. K. Uhlmann (1997). A New Extension of the Kalman Filter to Nonlinear Systems. Proceedings of the SPIE – The International Society for Optical Engineering, Vol 3068, April 1997, pp 182-193.

6. DeMars, K., M. Jah, D. Giza and T. Kelecy (2009). Orbit Determination Performance Improvements for High Area-to-mass Ratio Space Object Tracking using and Adaptive Gaussian Mixtures Estimation Algorithm, 21st International Symposium on Space Flight Dynamics (ISSFD), Toulouse, France, Sep-Oct 2009.

7. Shoemaker, M., B. Wohlberg and J. Koller (2013). Atmospheric Density Reconstruction Using Satellite Orbit Tomography Proceedings of the 23rd AAS/AIAA Space Flight Mechanics Meeting, Kauai, HI, Feb. 10-14, 2013.